Direct Evidence of Orbital Mixing between Water and Solvated Transition-Metal Ions: An Oxygen 1s XAS and DFT Study of Aqueous Systems

Lars-Åke Näslund,[†,‡] Matteo Cavalleri,[†] Hirohito Ogasawara,[†] Anders Nilsson,[†,§] Lars G. M. Pettersson,*[,†] Philippe Wernet,[§] David C. Edwards,[||] Magnus Sandström,[⊥] and Satish Myneni[#]

Fysikum, Alba Nova, and Structural Chemistry, Arrhenius Laboratory, Stockholm University, SE-10691 Stockholm, Sweden, Department of Physics, Uppsala University, P.O. Box 530, SE-75121 Uppsala, Sweden, Stanford Synchrotron Radiation Laboratory, P.O. Box 20450, Stanford, California 94309, and Departments of Chemistry and Geosciences, Princeton University, Princeton, New Jersey 08544

Received: February 4, 2003; In Final Form: June 12, 2003

We have studied the chemical bonding of water in the first hydration sphere to transition-metal ions in aqueous solutions by using X-ray absorption spectroscopy (XAS) combined with density functional theory calculations (DFT). The experimental technique is for the first time applied to the study of the oxygen K-edge absorption of liquid water in the presence of dissolved ions. We successfully resolved the electronic structure of water in the first hydration sphere. Features in the oxygen 1s XAS pre-edge region in Cr^{3+} and Fe^{3+} solutions are interpreted as mixing between the molecular orbitals of water and the open d shell of the transition-metal ion. These features are absent for Al^{3+} solutions. Effects on the electronic structure from anions in the first hydration sphere are also described.

1. Introduction

The essential role of water as a solvent in chemical processes is closely connected to the properties of the hydration spheres of aqua ions. The chemical interaction between the ion of an element and water as a ligand gives essential information not only on the aqueous chemistry of the element but also on the chemical properties of the element in general. For example, the vast differences in thermodynamics and kinetics of hydrated ions in aqueous solution when replacing a coordinated water molecule with another ligand or for the deprotonation of water ligands to give hydroxo species are controlled to some extent by the charge density on the central atom but also by electronic factors, in particular, ligand field effects for transition-metal ions.[1] Another factor of primary importance for the properties of aqueous solutions is the nature of the hydrogen bonding, which is strongly influenced by the presence of ions. It is well known that the conformation of proteins and nucleic acids, for example, the structure of DNA and its functions, depends on the nature of the ionic solution.[2]

Because of the importance of the ion−solvent interaction, a large number of experimental techniques, primarily EXAFS, X-ray, and neutron diffraction, have been applied to obtain direct structural information on the ion−water interaction. Structural and dynamic information is also available from NMR, infrared, and Raman spectroscopic methods as well as from theoretical calculations and computer simulations, but direct measurements of the local electronic structure of the water molecules in the solution have proven difficult. In surface science, near-edge X-ray absorption fine structure spectroscopy (NEXAFS, or more simply X-ray absorption spectroscopy, XAS)[3] is widely used to study the nature of the bonding between adsorbates and the surface. However, the extension to low-energy measurements at the oxygen K edge in aqueous solution has long been a challenge because of the high vapor pressure of the liquid. The requirement of a vacuum environment when the measurements are performed using electron detection has led to the construction and application of differentially pumped systems.[4] In those case, the measurements have typically been done on a thin film of liquid, which is constantly replenished. With the advent of third-generation synchrotron light sources, improved detection techniques, and the possibility to make ultrathin windows to separate the ultrahigh vacuum of the beamline from a high-pressure cell, measurements under ambient conditions have now become possible. Recently, we were able to apply high-resolution XAS to the oxygen K edge of liquid water using a fluorescent photon detection mode in a helium atmosphere.[5] The electronic structure of the liquid was compared to that in the solid state, which, in combination with theoretical calculations of spectra, lead to the spectroscopic identification of specific hydrogen-bonding situations.[5−7] In the present work, we will extend this analysis to specific effects on the electronic structure of water as a ligand to metal cations in aqueous solution.

XAS involves the excitation of a core electron into unoccupied orbitals. The experiments show chemical specificity because the core-level positions depend strongly on the element and are furthermore sensitive to the chemical environment. Finally, the extreme spatial localization of the core orbital involved in the transition makes X-ray absorption an extremely local probe of the electronic structure at a specific atomic site.

The excitation process obeys the dipole selection rule,[3] which for an atom strictly limits the change in the angular momentum quantum number (Δl) to ± 1. For K-shell transitions of molecular

* Corresponding author. E-mail: lgm@physto.se. Tel: +46 (8) 5537 8712. Fax: +46 (8) 5537 8442.
[†] Fysikum, Stockholm University.
[‡] Uppsala University.
[§] Stanford Synchrotron Radiation Laboratory.
[||] Department of Chemistry, Princeton University.
[⊥] Structural Chemistry, Stockholm University.
[#] Department of Geosciences, Princeton University.

10.1021/jp034296h CCC: $25.00
Published on Web 07/22/2003

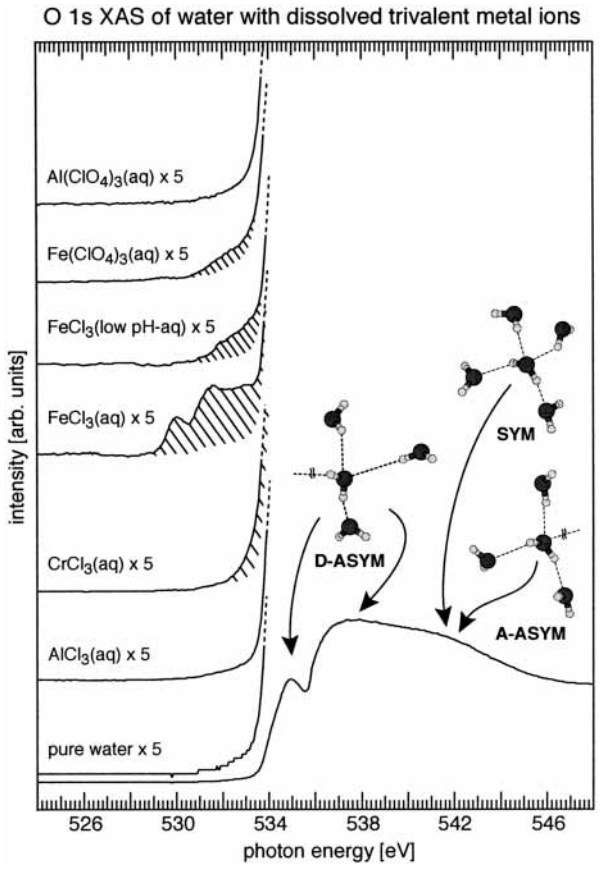

Figure 1. Experimental O 1s X-ray absorption spectrum of pure water showing a pre-edge peak assigned to asymmetric water molecules having one hydrogen bond broken at the donor side (D-ASYM).[5] Experimental O 1s X-ray absorption spectra of aqueous solutions showing extra pre-edge features (shaded area) but only if the dissolved trivalent metal ion is a transition element.

systems, the spatial localization of the 1s orbital involved in the excitation results in the spectrum being completely dominated by transitions to molecular orbitals with a local p-orbital contribution,[3] although the overall symmetry is not atomic-like. For an oxygen 1s electronic excitation, the features in the XAS spectrum will thus reflect only the local atomic p contribution to the excited orbital. Moreover, because of the short time scale of the excitation process (less than 1 fs, i.e. much faster than the vibrational and translational motions), the spectrum becomes the sum of snapshot contributions from individual molecules in their instantaneous environments.

In our earlier work we could, with the help of density functional theory (DFT) spectrum calculations for specific hydrogen-bonding situations, assign the XAS spectral features of the liquid to two different situations: (1) water molecules having one hydrogen bond broken at the donor side (D-ASYM) and (2) tetrahedral coordination (SYM) and unsaturation on the acceptor side (A-ASYM), where the latter two gave similar spectrum contributions (Figure 1). In the present paper, we will follow a similar strategy—combining XAS and DFT to study the local structure of water in transition-metal solutions. In particular, we will show that the molecular orbitals of water ligands in the first hydration sphere mix with the d orbitals of the metal ion, giving rise to low-intensity pre-edge features in the XAS spectrum. We propose that these features, which we have found for solutions of Cr^{3+} and Fe^{3+} but not for Al^{3+} (see Figure 1), are related to the electronic structure of the solvated trivalent transition-metal ions. Furthermore, we find these features to be sensitive to the composition of the first hydration sphere (e.g., the presence of inner-sphere chloride coordination as well as deprotonation of the water ligands give clear spectroscopic signals that serve to fingerprint these species).

2. Experimental Section

2.1. Experimental Technique. The oxygen 1s X-ray absorption spectroscopy (O 1s XAS) spectra were collected on beamline 8.0 at the Advanced Light Source (ALS) in Berkeley, CA. Because the method of detection is based on measuring fluorescence, it requires a high-flux undulator-based soft X-ray beamline. We have used the Soft X-ray Endstation for Environmental Research (SXEER) that makes it possible to separate the liquid under atmospheric pressure and room temperature in the sample chamber from the vacuum in the synchrotron beamline.[5] The chamber is filled with helium gas that is transparent to soft X-rays in the energy range of interest for O 1s XAS. Furthermore, by maintaining a constant flow of helium gas through the chamber, we continuously removed the water vapor; this is necessary because water vapor will contribute spectral features to the spectrum in the same energy range as liquid water. The XAS spectra are obtained in fluorescence mode, and the photons are detected with a GaAs photodiode. The spectra are normalized by the incident photon intensity, I_0, monitored with a gold mesh in the beamline. The I_0-normalized spectrum is also normalized with an XAS spectrum of the Si_3N_4 window that separates the helium atmosphere from the vacuum. This is necessary because of adsorbed water molecules on the window. The spectra are then calibrated with the peak photon absorption energy of the water vapor features (O 1s $\rightarrow 4a_1$ at 534.20 eV, O 1s $\rightarrow 2b_1$ at 536.10 eV, and O 1s $\rightarrow 2b_2$ at 537.25 eV), known from earlier experiments,[5] before subtracting the gas-phase contributions from the spectrum. Figure 2 demonstrates for pure water the steps involved to obtain the final XAS spectrum.

The geometry of the sample with respect to incoming and emitted X-rays is very important in order to avoid saturation effects, which arise when the detection depth is deeper than the absorption depth (i.e., when all photons are absorbed in the volume from which the fluorescence can escape and reach the detector). Saturation effects affect the spectra in the energy range where the intensity is high, and in the case of pure water, where the mean free path of the fluorescence is long, saturation effects may be present above 536 eV. The saturation effect can be reduced by maximizing the penetration depth of the X-ray beam and by minimizing the detection depth by letting the X-ray photons impinge the sample normal to the surface and then collecting the fluorescence at a grazing angle. To achieve such a geometry, the detector is placed perpendicular to the incoming photon beam, and a 0.4-mm slit is placed in front of the detector. The slit will screen off most of the fluorescence and give a detection angle of only 1−2°. Whether this arrangement is sufficient to eliminate the saturation effect completely in pure water is still under debate. In the present case, however, where metal chloride salts are dissolved in the water, the saturation effect is entirely eliminated by the present geometry because the chloride ions, with L-edge absorption, reduce the fluorescence mean free path in the sample. We will focus further on the origin of the low-intensity features below the pre-edge found for solutions containing transition-metal ions (Cr^{3+} and Fe^{3+}), and in that energy region, no saturation effects have been noticed even in the pure liquid water case. Thus, a comparison between the different spectra is valid in this energy region, whereas a discussion of the solvation-induced differences at higher energies, although highly interesting, must be investigated further.

2.2. Samples. The samples are prepared from commercially available salts from Sigma-Aldrich: chromium(III) chloride

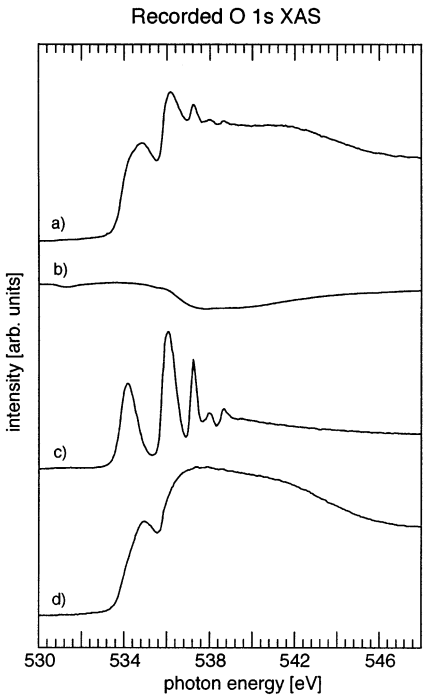

Figure 2. Recorded XAS spectra of (a) the sample, (b) the Si_3N_4 window, (c) water vapor, and (d) the result after normalization to the transmission function and the subtraction of gas-phase contributions. The spectrum from the sample has contributions from the water vapor in the He atmosphere. Normally, the peaks are smaller than shown, and it is possible to record spectra without water-vapor peaks. However, without the vapor peaks, it is difficult to do a photon energy calibration. There are also intensity variations due to absorption of the incoming light by the Si_3N_4 window. Furthermore, all spectra are normalized to the beamline transmission using a gold mesh prior to the Si_3N_4 window.

TABLE 1: Samples in the O 1s XAS Study of Aqueous Solutions of Trivalent Metal Ions $[M]^{3+}$(aq)

sample notation	$[M^{3+}]/m$	color at time of XAS
$AlCl_3$(aq)	0.89	colorless
$CrCl_3$(aq)	0.85	pale green
$Al(ClO_4)_3$(aq)	0.86	colorless
$Fe(ClO_4)_3$(aq)	0.84	pale yellow
$FeCl_3$(low pH, aq)	0.88	pale yellow
$FeCl_3$(aq)	0.87	yellow-brown

hexahydrate, $CrCl_3 \cdot 6H_2O$; aluminum chloride hexahydrate, $AlCl_3 \cdot 6H_2O$; iron(III) chloride hexahydrate, $FeCl_3 \cdot 6H_2O$, aluminum perchlorate, $Al(ClO_4)_3 \cdot 9H_2O$; and iron(III) perchlorate, $Fe(ClO_4)_3 \cdot 10H_2O$. The salts were dissolved in deionized water without any further preparation, except in the case of $FeCl_3$ (low pH, aq) where a few droplets of concentrated hydrochloric acid, HCl, are added before dissolving the salt. The sample notation, concentration, and color of the sample at the time of the XAS measurement are presented in Table 1.

2.3. Speciation. *Aluminum.* The small size of the Al^{3+} ion leads to extensive hydrolysis of its aqueous solutions, but at the high (~1 M) concentration of aluminum chloride hexahydrate, $AlCl_3 \cdot 6H_2O$(s), the dominating species is the hexaaquoaluminum ion $[Al(H_2O)_6]^{3+}$.[1,29]

Chromium. When chromium chloride hexahydrate, $CrCl_3 \cdot 6H_2O$(s), is dissolved in water, the solution will contain different species of Cr−Cl inner- and outer-sphere complexes. When fresh, the *trans*-dichlorotetraaquochromium(III) ion, $[CrCl_2(H_2O)_4]^+$, gives the solution a dark green color, but within 1 h, the solution gradually changes to light green because of the replacement of one of the chloride ligands by a water molecule.[8,9] The replacement of the second chloride ligand is a slow process and takes several days. Also, the hydrolysis is slow, and the dominant species will then become the violet hexaaquachromium(III) ion, $[Cr(H_2O)_6]^{3+}$.[9] In our experiments, we used a solution of $CrCl_3 \cdot 6H_2O$(s) that was ca. 24 h old and therefore had $[Cr(H_2O)_6]^{3+}$ and the monochloropentaaquochromium ion $[CrCl(H_2O)_5]^{2+}$ as the dominant species.[8]

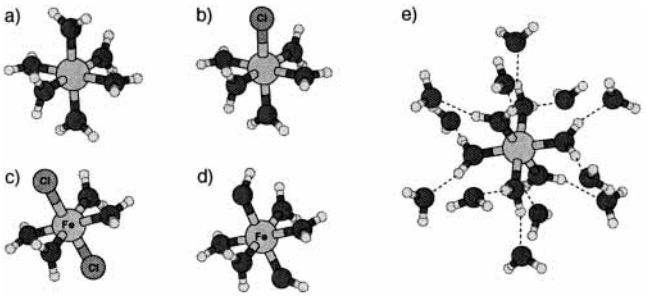

Figure 3. Structures of selected cluster models used in the DFT calculations: (a) $[M(H_2O)_6]^{3+}$, (b) $[MCl(H_2O)_5]^{2+}$, (c) $[FeCl_2(H_2O)_4]^+$, (d) $[Fe(OH)_2(H_2O)_4]^+$, and (e) $[M(H_2O)_{18}]^{3+}$ (M = trivalent metal ion).

Iron. There is a slow and complex set of hydrolysis polymerization processes in iron(III) solutions prior to the precipitation of iron(III) oxyhydroxides.[1] However, the formation of the first hydroxo complex $[Fe(OH)(H_2O)_5]^{2+}$ and the dimer $[Fe_2(OH)_2(H_2O)_8]^{4+}$ is rapid. Supersaturated solutions containing up to 10% of the dimer are reported to be stable with respect to the precipitation of goethite, α-FeOOH. Solutions of iron(III) chloride hexahydrate, $FeCl_3 \cdot 6H_2O$(s), will contain chloro complexes as well as particles of solid iron oxyhydroxides, which makes the spectra more difficult to analyze. By adding hydrochloric acid, HCl, before dissolving $FeCl_3 \cdot 6H_2O$(s), hydrolysis is suppressed, and the formation of chloro complexes is promoted. The dominating species will then be the dichlorotetraaquairon(III) ion, $[FeCl_2(H_2O)_4]^+$.[14,15] The first coordination sphere in $[FeCl_2(H_2O)_4]^+$ comprises four Fe−O bonds at around 2.0 Å and two Fe−Cl bonds at 2.3 Å.[15] In a solution of iron(III) perchlorate, $Fe(ClO_4)_3 \cdot 10\ H_2O$, the hexaaquaferric ion, $[Fe(H_2O)_6]^{3+}$, will dominate because the ClO_4^- ion, because of its very low coordinating ability,[10] will not influence the first hydration sphere.[11−13]

3. Theoretical Calculations

The interaction between the water molecules and the ion is described by means of molecular clusters, modeling the trivalent metal ion with its first hydration sphere. The simplest models of the isolated ion in water are $[M(H_2O)_6]^{3+}$ (M = trivalent metal ion), where the 6 water molecules bind to the cation octahedrally and $[M(H_2O)_{18}]^{3+}$, where the second solvation sphere, composed of 12 water molecules, is added (Figure 3). The use of the cluster approach is justified by the fact that the interaction of interest, between the water and the metal d orbitals, is very local in nature. The influence on the computed properties with respect to the hydration model was furthermore investigated by comparing results from these two cluster sizes (Figure 4). The two spectra appear to be very similar in the low-energy region (530−534 eV), where the discussion is focused in this paper, showing the high locality of the water−metal d interaction and justifying the use of the cluster approach in this case. The excited water molecule in the first solvation sphere has different local hydrogen bond structures in the two cases (the free OH bonds in the $[M(H_2O)_6]^{3+}$ model are instead coordinated by the second sphere of water molecules in the $[M(H_2O)_{18}]^{3+}$ cluster), which gives rise to the differences between the two spectra at

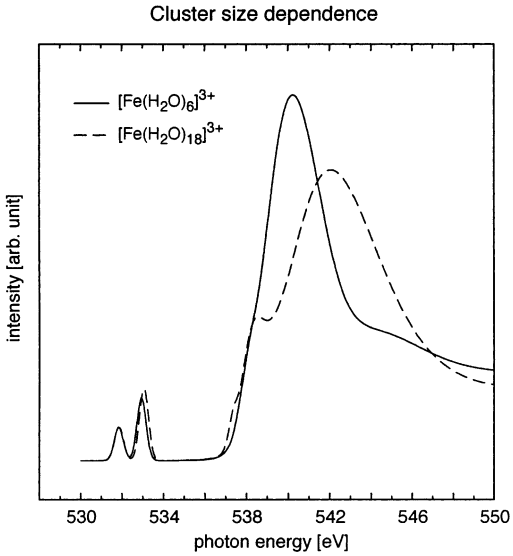

Figure 4. Calculated spectra of $[Fe(H_2O)_6]^{3+}$ (—) and $[Fe(H_2O)_{18}]^{3+}$ (– –) show that the interaction between the water molecule and the metal d orbitals is very local in nature and that the spectra of the two calculated cluster sizes do not differ in the low-energy region (530–535 eV). At higher energies, there are some differences because the excited water molecule in the first solvation sphere has a different local hydrogen bond structure in these two cases.

higher energies, especially in the pre-edge region, as described in our previous work on liquid water.[5−7]

Chloride ions can substitute water ligands in the first solvation sphere. Two chloro ligands in the octahedral $[MCl_m(H_2O)_{6-m}]^{(3-m)+}$ ($m = 1, 2$) clusters can occupy cis or trans positions, and all combinations were investigated. A more complex chemistry takes place in Fe(III) solution because of the high tendency of the ion to deprotonize the water molecules. These possibilities are studied by means of the $[Fe(OH)(H_2O)_5]^{2+}$ and $[Fe(OH)_2(H_2O)_4]^{1+}$ complexes, where the two hydroxyl groups that are formed can occupy both equatorial and axial positions in the distorted octahedron.[1] For all clusters, the experimental structure, determined in solution by EXAFS or neutron diffraction, is used if available,[8,16,17] and selected cluster structures are presented in Figure 3. For the remaining clusters, the geometries were optimized at the DFT/B3LYP level[18,19] using the Gaussian 98 program package.[20] For the geometry optimization, the standard 6-311G basis, with diffuse functions, was used for oxygen, hydrogen, chlorine, and aluminum, and the LANL2DZ pseudopotentials and basis sets were used to describe the transition metals.

The XAS spectra were generated within a DFT framework using the DeMon-StoBe program[21] with the exchange and correlation functionals developed by Becke,[22] Perdew, and Wang.[23] The spectral oscillator strengths (i.e., intensities) in X-ray absorption are obtained by computing the transition moment between the initial and final states.

$$I_{if} \propto |\langle \psi_i | \mu | \psi_f \rangle|^2 \quad (1)$$

Within the transition-potential approach,[24] the initial and the final states are obtained from the same wave function, characterized by a half-occupied core hole. The transition-element calculation for transition between the core level and an unoccupied orbital is thus simplified:

$$I_f \propto |\langle \phi_{1s} | \mu | \phi_f \rangle|^2 \quad (2)$$

This calculation results in a discrete set of energy levels, each associated with a specific oscillator strength. The obtained oscillator strengths are then convoluted with Gaussians of linearly increasing full width at half-maximum (fwhm) to obtain the spectra. Effective core potentials (ECP),[25] eliminating the O 1s level on all oxygen atoms but the core-excited one, were used to simplify the definition of the core hole. The core-excited oxygen was described using the IGLO-III all-electron basis set of Kutzelnigg et al.[26] For the chlorine and metal atoms, TZVP and DZVP all-electron basis sets[27] were used, respectively. The calculations were performed using a double basis set technique where in the spectrum calculation the normal molecular basis is augmented by a large diffuse basis (~150 functions) to improve the description of the Rydberg and continuum states.[28]

4. Results and Discussion

With the experimental setup described in the Experimental Section, we were recently able to probe the electronic structure in liquid water successfully by using XAS at the oxygen K edge.[5] An experimental O 1s XAS spectrum of pure water[5] is presented in Figure 1, and the spectral features (the strong pre-edge peak at 535 eV, an enhancement at 537 eV, and a less pronounced structure at 542 eV compared to bulk ice) were shown to be sensitive to the specific bonding of the hydrogens (donating H-bond) but not of the oxygen lone pair. The reason for this is that XAS measures the unoccupied 2p character at the oxygen of the probed water molecule, which gives a very low intensity for excitations involving the essentially doubly occupied lone pairs. Three different bonding situations of the water molecules were considered in ref 5: saturated fully coordinated (SYM), unsaturated with a missing hydrogen bond at the acceptor side (A-ASYM), and unsaturated with a missing hydrogen bond at the donor side (D-ASYM). Because the SYM and A-ASYM species were found to give similar contributions to the spectrum, we can distinguish spectroscopically only whether the H-bonding at the hydrogen side is saturated. The results in the previous work indicate that the unsaturated donating H-bonding environment applies to a dominating fraction of the water molecules.

O 1s XAS spectra of aqueous solutions of metal ions have overall similar features to those of pure water. There are small changes in the intensities and the peak positions, showing that the metal ions affect the H-bonding in water. In the present paper, however, we will focus our interest on the new features that appear in the pre-edge region of the O 1s XAS spectra of aqueous solutions of transition-metal ions. (See the shaded areas in Figure 1.) In $FeCl_3$(aq), there are extra features that are not present in pure water. New features are also present in $FeCl_3$(low pH, aq) and $Fe(ClO_4)_3$(aq), but they not as clear as those in the $FeCl_3$(aq) solution, and in $CrCl_3$(aq), the pre-edge seems to be slightly shifted to lower energy. The aluminum(III) solutions, $Al(ClO_4)_3$(aq) and $AlCl_3$(aq), do not show any major differences from pure water. Because these features appear in aqueous solutions of Fe^{3+} and Cr^{3+} but not Al^{3+}, they should be related to the electronic structure of the transition-metal ions and the specific bonding in their coordination sphere.

The d orbitals are strongly influenced by the surrounding ion. The hexaaquochromium ion $[Cr(H_2O)_6]^{3+}$ is the most inert hydration complex of the first-row trivalent transition-metal ions mainly because of its large ligand-field activation energy.[14,29] In the current experiment, we can expect that a certain amount of the monochloro complex, $[CrCl(H_2O)_5]^{2+}$, is present in addition to the hexaaquochromium ion, $[Cr(H_2O)_6]^{3+}$. The inner-sphere chloro ligand in the $[CrCl(H_2O)_5]^{2+}$ complex can have

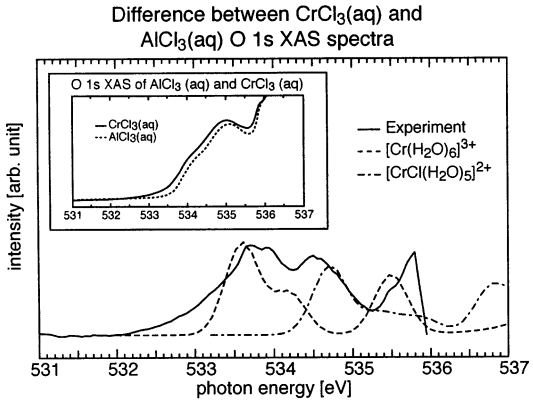

Figure 5. (Inset) Experimental O 1s XAS spectrum of $CrCl_3$(aq) (—) and $AlCl_3$(aq) (− −). Features in the difference spectrum between $CrCl_3$-(aq) and $AlCl_3$(aq) (—) and in the calculated spectrum of $[Cr(H_2O)_6]^{3+}$ (− −) and $[CrCl(H_2O)_5]^{2+}$ (− · −) serve as spectroscopic proof of d-orbital interaction between the Cr^{3+} ion and the water molecules in the first hydration sphere. In the case of the computed $[CrCl(H_2O)_5]^{2+}$, the spectra is the sum of the contributions of core excitations from water molecules in equatorial and axial positions in the distorted octahedra, with chlorine occupying the remaining axial position.

some effect on the XAS spectra, which will be analyzed on the basis of the theoretical calculations below.

The main-group Al^{3+} metal ion with the closed-shell [Ne] electronic configuration binds the first-sphere water molecules octahedrally with almost the same metal−oxygen distance as Cr^{3+}: 1.88 and 1.96 Å, respectively. (The size of the water ligand is 1.34 Å.[29,30]) For both ions, the mean metal ion−oxygen distance to the second solvation sphere is about 4.0−4.2 Å.[8,9,11,29,31−35] The geometrical differences in the hydration spheres of the cations are thus small enough that the comparison should provide useful information pertaining mainly to the differences in electronic structure.

Experimental O 1s XAS spectra of water with dissolved aluminum chloride, $AlCl_3$(aq), and water with dissolved chromium chloride, $CrCl_3$(aq), are shown in the inset of Figure 5, covering the energy range of 531−536 eV. (Note the more extended energy range than that shown in Figure 1.) It is clearly seen that $AlCl_3$(aq) has a double pre-edge peak with a shoulder at 534.3 eV and maximum at 535.1 eV that differs from the spectrum of pure water, presented in Figure 1. The present interpretation is that this difference is due to changes in the distribution of the D-ASYM water species in the bulk caused by the ion hydration. $CrCl_3$(aq) has the same feature but shifted to lower energy by 0.1 eV. This is actually not a shift in peak position but a shift due to extra features in the energy range of 532−536 eV. Because the new features in $CrCl_3$(aq) appear very close to the pre-edge, we have used a subtraction procedure to enhance them. A difference spectrum between the $CrCl_3$(aq) spectrum and the $AlCl_3$(aq) spectrum is presented in Figure 5 showing three peaks at 533.8, 534.5, and 535.8 eV. The computed spectrum for the $[Cr(H_2O)_6]^{3+}$ cluster is compared with the experimental difference spectrum in the Figure. It is clear that the two features at 533.8 and 535.8 eV are well reproduced by the computed spectrum. To assign the feature at 534.5 eV, we turn to the computed spectra of chloro complex $[CrCl(H_2O)_5]^{2+}$, also shown in Figure 5, where we consider the inclusion of one chloride in the first solvation sphere (Figure 3). We find that the chloro ligand induces an upward shift of the spectrum by about 1 eV as well as a slight compression of the features. The comparison with experiment suggests that the feature at 534.5 eV should be assigned to the t_{2g} component of the $[CrCl(H_2O)_5]^{2+}$ complex. The corresponding e_g component

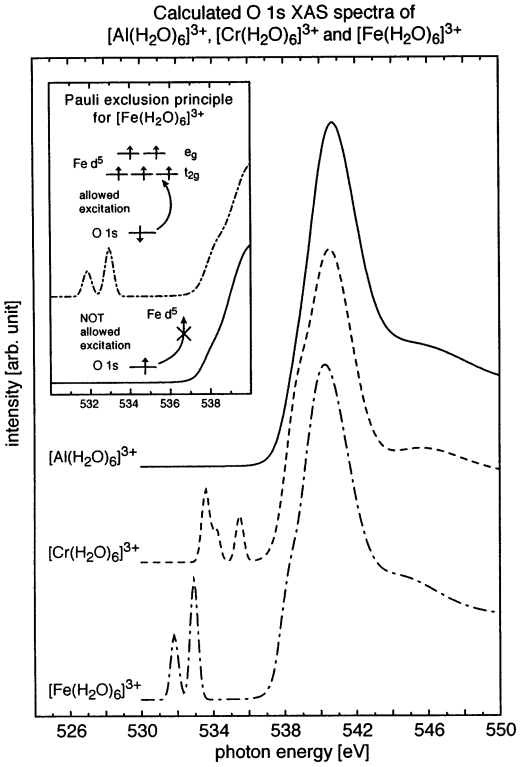

Figure 6. Calculated O 1s X-ray absorption spectra of $[Al(H_2O)_6]^{3+}$ (—), $[Cr(H_2O)_6]^{3+}$ (− −), and $[Fe(H_2O)_6]^{3+}$ (− · −) clusters. The computed spectra are the sum of the O 1s parallel spin and O 1s antiparallel spin XAS spectra as the example in the inset illustrates. The inset shows that only electrons with antiparallel spin are allowed to contribute to excitations to the water molecular orbitals that are mixing with the open d shell of the transition-metal ion. The structures involving the d orbitals in the energy region of 530−536 eV change with the anion, but the structures at higher energies are less sensitive.

is then shifted up into the energy region masked by the dominating bulk contributions. Also, in the case of computed iron complexes where one or two chlorines replace water molecules in the first solvation sphere, the same upward shift together with a reduction in intensity of the first t_{2g} component is noticed (see below).

Figure 6 compares the calculated O 1s XAS spectrum of the hexacoordinated Al^{3+}, Cr^{3+}, and Fe^{3+} ions. We can see that the $[Al(H_2O)_6]^{3+}$ spectrum does not display any features in the energy range of 529−536 eV, whereas $[Cr(H_2O)_6]^{3+}$ and $[Fe(H_2O)_6]^{3+}$ show three and two peaks, respectively. In aqueous solution, the hydrated chromium and iron ions form octahedrally coordinated high-spin complexes[1] with singly occupied t_{2g} and e_g orbitals. This leads, in the case of Cr^{3+}, to an electronic structure ($[Ar]3d^3$) where the three electrons in the d orbitals have parallel spin. The case of aqueous Fe^{3+} ($[Ar]3d^5$) is characteristic of the small crystal-field splitting of the first-row transition-metal ions because the five outer electrons can occupy all of the d orbitals without pairing. In this way, an O 1s electron, with spin antiparallel to that of the five d electrons, can be excited into an iron d orbital, but this transition will be "Pauli-forbidden" for an electron with parallel spin (Figure 6 inset). Excitations from both O 1s spin orbitals must thus be considered to generate the spectra. This fact will furthermore be useful in assigning features in the computed XAS spectra to transitions involving excitation into the metal d orbitals, so for each cluster, two distinct spectrum calculations are performed: with the spin of the excited O 1s electron parallel and antiparallel to that of the d electrons in the trivalent ion. An excitation of an antiparallel-spin core electron into the d orbitals will give rise

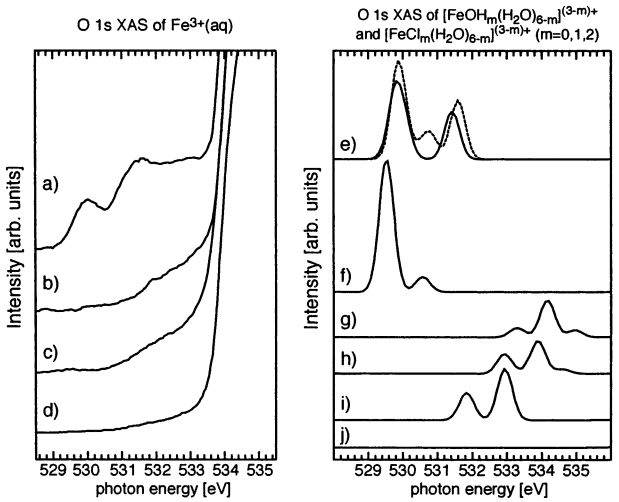

Figure 7. Experimental O 1s X-ray absorption spectra of (a) $FeCl_3$(aq), (b) $FeCl_3$(low pH, aq), (c) $Fe(ClO_4)_3$(aq), and (d) $AlCl_3$(aq) compared to computed spectral features of hydrated chloro and hydroxo iron(III) clusters (e) $[FeOH_{ax}OH_{ax}(H_2O)_4]^+$ (—), $[FeOH_{ax}OH_{eq}(H_2O)_4]^+$ (— —), (f) $[FeOH(H_2O)_5]^{2+}$, (g) $[FeCl_2(H_2O)_4]^+$, (h) $[FeCl(H_2O)_5]^{2+}$, (i) $[Fe(H_2O)_6]^{3+}$, and (j) $[Al(H_2O)_6]^{3+}$. The technique is sensitive enough to distinguish changes in the first hydration sphere of the metal ion.

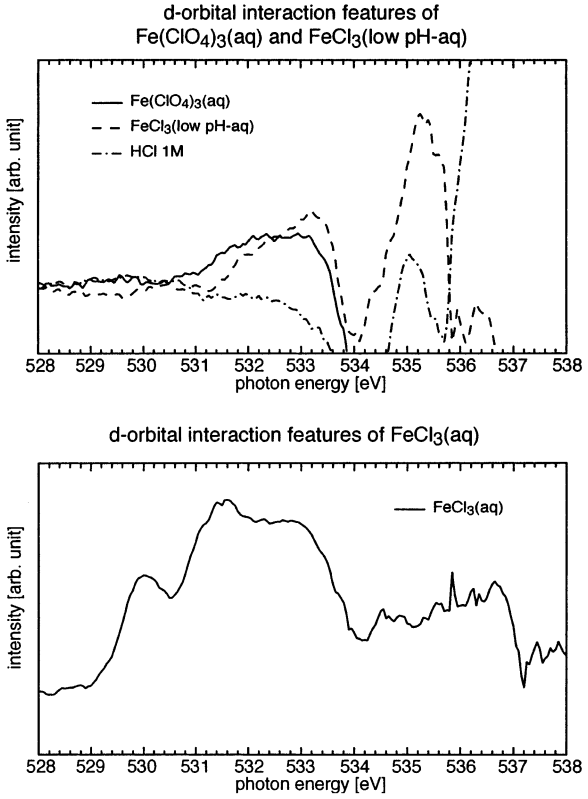

Figure 8. Differential O 1s X-ray absorption spectra between (top) $Fe(ClO_4)_3$(aq) and $Al(ClO_4)_3$(aq) (—), $FeCl_3$(low pH, aq), and $AlCl_3$(aq) (— —), 1 M HCl(aq) and pure water (— · —), and (bottom) $FeCl_3$(aq) and $AlCl_3$(aq). The d interaction peak is shifted to higher energy in $FeCl_3$(low pH, aq) because of the chloro ligands in the hydration sphere. The strong features in the O 1s XAS of $FeCl_3$(aq) are due to OH ligands in a colloidal precipitate.

to two peaks in the XAS spectrum. In the case of a parallel-spin core-electron excitation, the transition into the 3d orbitals is forbidden in the Fe^{3+} ion, but it is allowed for Cr^{3+} because of its d^3 configuration. The two e_g orbitals in the Cr^{3+} ion are completely empty and free for excitation of both parallel and antiparallel-spin core electrons.

From a simple consideration of the number of empty t_{2g} and e_g levels, one would expect corresponding intensity ratios of 3:2 for Fe^{3+} and 3:4 for Cr^{3+}; these are not obtained from the calculations. To understand this, it must be remembered that the ligand-field splitting of the t_{2g} and e_g levels is due to the interaction with the oxygen lone pairs of the coordinated water molecules. The e_g orbitals are pointing against the oxygen lone pairs, but the t_{2g} orbitals are not, resulting in different interactions. If we anticipate that the observed orbitals are antibonding, we can expect that the more strongly interacting e_g will be at higher energy and contain a larger water contribution. This will lead to the observed energy splitting and a larger intensity for the e_g interacting orbitals in the spectra. Hence, the intensity ratios of the d-orbital interaction-derived features are different than expected. The extra, low-energy features, as can be seen in Figures 5 and 6, can originate only from the d-orbital interactions between the water molecules and the trivalent d-metal ion. Finally, the energy shift of about 2 eV between the d-orbital interaction features of the $[Cr(H_2O)_6]^{3+}$ and the $[Fe(H_2O)_6]^{3+}$ clusters is due to the different energy of the d levels in Cr and Fe where the higher nuclear charge of the Fe atom leads to a greater stabilization and thus a lower energy for transitions into the 3d levels of Fe^{3+}.

To show that the mixing between the molecular orbitals of water and the Cr^{3+} d orbitals represents a general case in all transition metals, we have also studied aqueous iron(III) solutions. Figure 7 (left) includes the experimental O 1s XAS spectra of $FeCl_3$(aq), $Fe(ClO_4)_3$(aq), and $FeCl_3$(low pH, aq). As compared to $Fe(ClO_4)_3$(aq) or $FeCl_3$(low pH, aq), the shapes of the d-orbital features are more distinct in the $FeCl_3$(aq) spectrum but also more complicated. The difference between the $FeCl_3$(aq) and $AlCl_3$(aq) spectra (Figure 8 , bottom) displays local maxima at 530.0, 531.6, and 532.8 eV. Figure 7 (right) shows the computed X-ray absorption spectrum of oxygen in the OH^- ligands of the $[Fe(OH)(H_2O)_5]^{2+}$ and $[Fe(OH)_2(H_2O)_4]^+$ clusters (Figure 3). The agreement indicates that the first peaks in the $FeCl_3$(aq) spectrum, at 530.0 and 531.6 eV, respectively, are due to the interaction between the OH^- molecular orbitals and the d orbitals in the metal. A confirmation of this is the absence of these two peaks in the experimental spectra of the $FeCl_3$ solution at low pH (Figure 7, left). The broad peak at 532.9 eV is then assigned to the d interaction of the water molecules in the Fe^{3+} ion solvation sphere. The yellow-brown color of the $FeCl_3$(aq) solution indicated that a colloidal precipitate had formed to some extent. Equilibrium calculations indicate that a substantial fraction of the iron would be present in amorphous iron(III) hydroxides or crystalline solid compounds such as $Fe(OH)_{2.7}Cl_{0.3}$(s) and that the dominating solution species would be $[FeCl_2(H_2O)_4]^+$ and $[FeCl(H_2O)_5]^{2+}$. Thus, it is likely that the observed features are due to the hydroxo groups in the solid precipitates.

By adding HCl to the iron(III) chloride solution to prevent the precipitation of iron(III) (oxy)hydroxides, the speciation will be simplified, and hydrolysis is suppressed. The experimental O 1s XAS spectrum of water with dissolved ferric chloride at low pH, $FeCl_3$(low pH, aq), is shown in Figure 7 (left). The features in the energy range of 531−534 eV look similar to those for the aqueous iron(III) perchlorate solution, $Fe(ClO_4)_3$(aq), but are somewhat shifted to higher energy. Calculations in Figure 7 (right) showing the theoretical spectrum of the $[Fe(H_2O)_6]^{3+}$, $[FeCl(H_2O)_5]^{2+}$, and $[FeCl_2(H_2O)_4]^+$ complexes indicate that the presence of the chloro ligands in the first solvation sphere is responsible for the shift to higher energy of the d-orbital-derived features.

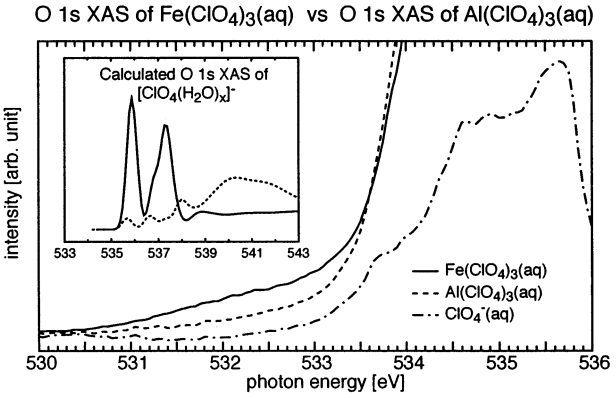

Figure 9. Difference curve between the $Al(ClO_4)_3$(aq) and $AlCl_3$(aq) spectra (− · −) shows that the perchlorate oxygen will not contribute in the energy range of the d-orbital interaction features. DFT calculations (inset) of $O_3ClO(1s)\cdots H_2O$ K-edge (—) and $ClO_4\cdots H_2O(1s)$ K-edge (− −) support the experimental results.

To ensure that the addition of hydrochloric acid does not produce new features in the region of interest, a difference spectrum between 1 M HCl(aq) and pure water is also shown together with the $FeCl_3$(low pH, aq) difference spectrum in Figure 8 (top). The HCl(aq) difference spectrum shows a structure at 535.1 eV, but the region below 535 eV is not affected. The difference between the $FeCl_3$(low pH, aq) and $AlCl_3$(aq) spectra actually has a peak at 535.3 eV that could originate from excess hydrochloric acid as in HCl(aq).

The experimental O 1s XAS spectrum of water with dissolved iron(III) perchlorate, $Fe(ClO_4)_3$(aq), is shown in Figure 7 (left). There is, as for $CrCl_3$(aq), an extra feature in the pre-edge region. The oxygen atoms in the ClO_4^- ion will also be excited and give features in the XAS spectra, but not in the area of interest for the d-orbital interaction and will not affect our analysis (Figure 9.) To ascertain that there are no intensity contributions from the oxygens of the counterion in the lower-energy region of the spectra, the $Fe(ClO_4)_3$(aq) spectrum is compared to an O 1s XAS spectrum of water with dissolved aluminum perchlorate, $Al(ClO_4)_3$(aq). Calculations of XAS spectra for the ClO_4^- ion also show that the perchlorate does not give any contribution in the region below 535 eV (Figure 9 inset). A difference spectrum of $Al(ClO_4)_3$(aq) and $AlCl_3$(aq) showing the ClO_4^-(aq) contribution to the spectrum supports the conclusions from the calculations, as shown in Figure 9. The features at 530.5−533.5 eV must then be due to the interaction between the water molecule and the d orbitals in the Fe^{3+} ion.

The difference between the $Fe(ClO_4)_3$(aq) and $Al(ClO_4)_3$(aq) spectra is shown in Figure 8 (top) together with the corresponding difference between the $FeCl_3$(low pH, aq) and $AlCl_3$(aq) spectra. The first difference curve displays d-orbital structure from 531 to 533.6 eV, and the second shows d-orbital structure from 531.3 to 533.7 eV. The shape is somewhat different; $Fe(ClO_4)_3$(aq) has rather uniformly distributed features of the d-orbital structure, but $FeCl_3$(low pH, aq) has more intensity at higher energy. This experimental evidence further supports our assertion that the shift to higher energy is due to the presence of chloro ligands in the inner solvation sphere of Fe^{3+}.

5. Conclusions

In this work, we have demonstrated the utility of X-ray absorption spectroscopy, in combination with DFT calculations of the spectral contributions, in studying the electronic structure of water in the first hydration sphere of metal ions. In our study, we focused our attention on the interaction between M^{3+} transition-metal ions and the water molecules in their first solvation sphere, resulting in characteristic peaks in the O 1s XAS spectral pre-edge region. In particular, the peaks below 536 eV in the spectra of Cr(III) and Fe(III) aqueous solutions but missing in the case of Al(III) provide evidence for the existence of orbital mixing between the d orbitals of the metals and the molecular orbitals of the solvating water. This interaction between the water and the metal d orbitals is certainly anticipated in the literature,[36] even though direct experimental electronic structure proof is missing. In fact, no technique other than XAS, combined with DFT calculations, is sensitive and selective enough to use as a direct experimental probe of the local orbital changes resulting from such a weak interaction.

Moreover, XAS shows great sensitivity to the local environment of the solvated metal ion, and the formation of metal−chlorine inner-sphere complexes is fingerprinted by a chemical shift in the position of the d-orbital interaction-derived features.

In the case of the complex $FeCl_3$(aq) solution, the peaks located in the 530−532 eV region could be assigned to the excitation of the oxygens in the hydroxyl groups resulting from the hydrolysis of water molecules and the probable formation of $Fe(OH)_{2.7}Cl_{0.3}$(s) solid precipitates.

In addition to the pre-edge region, aqueous solution XAS spectra also differ slightly from the pure bulk water spectrum at higher energies. Although we did not focus on this part of the spectra in the present work, the information contained there is indeed interesting and will be the aim of further investigations.

Combined XAS-DFT is a powerful tool for providing insight into the local electronic structure of a hydrogen-bonded liquid, and we successfully applied it for the first time on water,[5,6] showing a great sensitivity to the symmetry and the saturation of the local hydrogen bond structure. Now this technique is extended to the case of transition-metal aqueous solution, and for its unique capacity of probing the local electronic structure around the central ion, it holds the promise of becoming an important tool, in addition to EXAFS and neutron and X-ray diffraction, for the study of aqueous solutions in chemistry, biology, and environmental science.

Acknowledgment. The experimental part of this research is supported by the Basic Energy Sciences (Geosciences, Department of Energy, USA), the Swedish Royal Academy of Science (KVA), Göran Gustafsson's Foundation for Research in Natural Science and Medicine, and the National Science Foundation (U.S.) under grant CHE-0089215. The theoretical part of this investigation is supported by the Swedish Natural Science Research Council (NFR), the Foundation for Strategic Research, and the Swedish Center for Parallel Computing (PDC). The Advanced Light Source is supported by the Director, Office of Science, Office of Basic Energy Sciences, Material Sciences Division of the U.S. Department of Energy under contract no. DE-AC03-76SF00098 at Lawrence Berkeley National Laboratory. Portions of this research were carried out at the Stanford Synchrotron Radiation Laboratory, a national user facility operated by Stanford University on behalf of the U.S. Department of Energy, Office of Basic Energy Sciences.

Note Added after ASAP Posting. Because of a production error, this article was posted ASAP on 7/22/2003 with errors in the reference numbers. The correct version was posted on 7/24/2003.

References and Notes

(1) Richens, D. T. *The Chemistry of Aqua Ions*; Wiley and Sons: Chichester, U.K., 1997; Chapter 1.

(2) Saeger, W. *Principles of Nucleic Acid Structure*; Springer-Verlag: New York, 1983.
(3) Stöhr, J. *NEXAFS Spectroscopy*; Springer-Verlag: Berlin, 1992.
(4) Siegbahn, H.; Svensson, S.; Lundholm, M. *J. Electron Spectrosc. Relat. Phenom.* **1981**, *24*, 205. Siegbahn, H. *J. Phys. Chem.* **1985**, *89*, 897. Lundholm, M.; Siegbahn, H.; Holmberg, S.; Arbman, M. *J. Electron Spectrosc. Relat. Phenom.* **1986**, *40*, 163.
(5) Myneni, S.; Luo, Y.; Näslund, L-Å.; Cavalleri, M.; Ojamäe, L.; Ogasawara, H.; Pelmenschikov, A.; Wernet, Ph.; Väterlein, P.; Heske, C.; Hussain, Z.; Pettersson, L. G. M.; Nilsson, A. *J. Phys.: Condens. Matter* **2002**, *14*, L213.
(6) Wilson, K. R.; Cavalleri, M.; Rude, B. S.; Schaller, R. D.; Nilsson, A.; Pettersson, L. G. M.; Goldman, N.; Catalano, T.; Bozek, J. D.; Saykally, R. J. *J. Phys.: Condens. Matter* **2002**, *14*, L221.
(7) Cavalleri, M.; Ogasawara, H.; Pettersson, L. G. M.; Nilsson, A. *Chem. Phys. Lett.* **2002**, *364*, 363
(8) Díaz-Moreno, S.; Muñoz-Páez, A.; Martinez, J. M.; Pappalardo, R. R.; Marcos, E. S. *J. Am. Chem. Soc.* **1996**, *118*, 12654.
(9) Magini, M. *J. Chem. Phys.* **1980**, *73*, 2499.
(10) Bailar, J. C.; Emeléus, H. J.; Nyholm, R.; Trotman-Dickenson, A. F. *Comprehensive Inorganic Chemistry*, 1st ed; Pergamon Press: Elmsford, NY, 1973.
(11) Lindqvist-Reis, P.; Muñoz-Páez, A.; Díaz-Moreno S.; Pattanaik, S.; Persson I.; Sandström, M. *Inorg. Chem* **1998**, *37*, 6675.
(12) Magini, M. *J. Inorg. Nucl. Chem.* **1978**, *40*, 43.
(13) Herdman, G. J.; Neilson, G. W. *J. Phys.: Condens. Matter* **1992**, *4*, 627.
(14) Cotton, F. A.; Wilkinson, G. *Advanced Inorganic Chemistry*, 5th ed.; Wiley & Sons: New York, 1998.
(15) Magini, M. *J. Chem. Phys.* **1979**, *71*, 4255.
(16) Morrison, T. I.; Reis, A. H.; Knapp, G. S.; Fradin, F. Y.; Chen, H.; Klippert, T. E. *J. Am. Chem. Soc.* **1978**, *100*, 3262.
(17) Hashimoto, S.; Forster, K.; Moss, S. C. *J. Appl. Crystallogr.* **1989**, *22*, 173.
(18) Becke, A. D. *J. Chem. Phys.* **1993**, *98*, 5648.
(19) Lee, C.; Yang, W.; Parr, R. G. *Phys. Rev. B* **1988**, *37*, 785.
(20) Frisch, M. J.; Trucks, G. W.; Schlegel, H. B.; Scuseria, G. E.; Robb, M. A.; Cheeseman, J. R.; Zakrzewski, V. G.; Montgomery, J. A., Jr.; Stratmann, R. E.; Burant, J. C.; Dapprich, S.; Millam, J. M.; Daniels, A. D.; Kudin, K. N.; Strain, M. C.; Farkas, O.; Tomasi, J.; Barone, V.; Cossi, M.; Cammi, R.; Mennucci, B.; Pomelli, C.; Adamo, C.; Clifford, S.; Ochterski, J.; Petersson, G. A.; Ayala, P. Y.; Cui, Q.; Morokuma, K.; Malick, D. K.; Rabuck, A. D.; Raghavachari, K.; Foresman, J. B.; Cioslowski, J.; Ortiz, J. V.; Stefanov, B. B.; Liu, G.; Liashenko, A.; Piskorz, P.; Komaromi, I.; Gomperts, R.; Martin, R. L.; Fox, D. J.; Keith, T.; Al-Laham, M. A.; Peng, C. Y.; Nanayakkara, A.; Gonzalez, C.; Challacombe, M.; Gill, P. M. W.; Johnson, B. G.; Chen, W.; Wong, M. W.; Andres, J. L.; Head-Gordon, M.; Replogle, E. S.; Pople, J. A. *Gaussian 98*, revision A.7; Gaussian, Inc.: Pittsburgh, PA, 1998.
(21) Principal authors: Casida, M. E.; Daul, C.; Goursot, A.; Hermann, K.; Koester, A.; Pettersson, L. G. M.; Proynov, E.; St-Amant, A.; Salahub, D. R. Contributing authors: Carravetta, V.; Duarte, H.; Godbout, N.; Guan, J.; Jamorski, C.; Leboeuf, M.; Malkin, V.; Malkina, O.; Nyberg, M.; Pedocchi, L.; Sim, F.; Triguero, L; Vela, A. *deMon-KS StoBe*, version 1.0.; deMon Software, 2001.
(22) Becke, A. D. *Phys. Rev. A* **1988**, *38*, 3098.
(23) Perdew, J. P. *Phys. Rev. B* **1986**, *34*, 7406.
(24) Triguero, L.; Pettersson, L. G. M.; Ågren, H. *Phys. Rev. B* **1998**, *58*, 8097.
(25) Pettersson, L. G. M.; Wahlgren, U.; Gropen, O. *J. Chem. Phys.* **1987**, *86*, 2176.
(26) Kutzelnigg, W.; Fleischer, U.; Schindler, M. *NMR: Basic Principles and Progress*; Springer-Verlag: Heidelberg, Germany, 1990.
(27) Huzinaga, S.; Andzelm, J. In *Gaussian Basis Sets for Molecular Calculations*; Huzinaga, S., Ed.; Elsevier: Amsterdam, 1965. Huzinaga, S.; Andzelm, J. *J. Chem. Phys.* **1984**, *42*, 1293.
(28) Ågren, H.; Carravetta, V.; Vahtras, O.; Pettersson, L. G. M. *Theor. Chem. Acc.* **1997**, *97*, 14.
(29) Helm, L.; Merbach, A. E. *Coord. Chem. Rev.* **1999**, *187*, 15.
(30) Beattie, J. K.; Best, S. P.; Skelton, B. W.; White, A. H. *J. Chem. Soc., Dalton Trans.* **1981**, 2105.
(31) Bol, W.; Welzen, T. *Chem. Phys. Lett.* **1977**, *49*, 189.
(32) Read, M. C.; Sandström, M. *Acta Chem. Scand.* **1992**, *46*, 1177.
(33) Merkling, P. J.; Muñoz-Páez, A.; Pappalardo, R. R.; Marcos, E. S. *Phys. Rev. B* **2001**, *64*, 092201-1.
(34) Caminiti, R.; Licheri, G.; Piccaluga, G.; Pinna, G. *J. Chem. Phys.* **1979**, *71*, 2473.
(35) Caminiti R.; Radnai T. *Z. Naturforsh., A* **1980**, *35*, 1368.
(36) Davy, R. D.; Hall, M. B. *Inorg. Chem.* **1988**, *27*, 1417.